A tyre-rim interaction digital twin for biaxial loading conditions

Mechanism and Machine Theory 191 (2024) 105491

Contents lists available at ScienceDirect

Mechanism and Machine Theory

journal homepage: www.elsevier.com/locate/mechmt

Research paper

A tyre-rim interaction digital twin for biaxial loading conditions

Simone Venturini *, Elvio Bonisoli, Carlo Rosso, Mauro Velardocchia

Politecnico di Torino, Department of Mechanical and Aerospace Engineering, Corso Duca degli Abruzzi, 24, Torino 10129, Italy

ARTICLE INFO

Keywords:
Biaxial test bench
Tyre-rim interface
Imposed kinematics
Overturning moment

ABSTRACT

This paper proposes a digital twin of automotive steel wheel biaxial test bench for wheel dynamic behaviour and assessment condition purposes. The methodology allows to consider the imposed kinematics occurring in the experimental test bench after the calibration process called "Overturning Moment procedure" is applied, and to manage the pneumatic tyre-rim interactions using finite element method decoupled models of the tyre and the wheel. The proposed scheme depicts the main loading contributions and introduces linearisation to improve the computational efficiency. The standard requirements, the Original Equipment Manufacturer specifications, and the working principle of the test bench are discussed. Hence, a comprehensive view of the physical behaviour of the introduced hypotheses in the digital twin development is presented. The reliability of the approach is validated against an industrial case study with numerical-experimental comparisons of the optimal camber angle and stress analysis.

1. Introduction

The overall performance of the vehicle heavily relies on the wheel's behaviour, which plays a crucial role in various essential functions, such as supporting the vehicle's weight and absorbing impact forces from the ground. Additionally, it facilitates the transmission of rotary motion from the axles to the tyres [1,2], while also ensuring driving stability [3], safety, and comfort [4].

To ensure the reliability of both the tyre and wheel, it is necessary to conduct tests in laboratory settings which replicate accelerated real-world loading conditions. In Europe, ISO 3894:2023, together with the European Tyre and Rim Technical Organisation (E.T.R.T.O) standard [5,6], mandate consistent tyre and wheel dimensions, material compliance, and test requirements for passenger car and truck wheels, as the biaxial fatigue test [7]. Three different biaxial test machine configurations are available [7], in which camber angle and loading condition ranges vary.

The design philosophy of the automotive wheel component primarily focuses on optimizing its geometry to achieve lightweight solutions [1]. It is imperative that the design exhibits fail-safe characteristics when subjected to fatigue tests, encompassing all potential combinations of tyre-wheel coupling scenarios. As a result, the prevailing design strategy relies on an iterative process of refining wheel features, followed by rigorous validation using experimental test benches. This validation procedure heavily relies on extensive and time-consuming fatigue tests.

The recent abrupt development automotive field and the request of reduction of component development time brought to the heavy integration of Digital Twin (DT) in the automotive field. A DT is a virtual replica or representation of a physical object, system, or process. It encompasses a combination of simulation, modelling techniques, and real system data to create a comprehensive digital counterpart that mirrors the characteristics, behaviour, and attributes of its physical counterpart. DT enable analysis, optimization,

* Corresponding author.
E-mail address: simone.venturini@polito.it (S. Venturini).

https://doi.org/10.1016/j.mechmachtheory.2023.105491
Received 18 July 2023; Received in revised form 13 September 2023; Accepted 14 September 2023

and eventually real-time monitoring of physical assets and processes, offering valuable insights for decision-making, predictive maintenance, performance optimization, and design improvements [8]. In 2019, Biesinger et al. performed a survey identifying the necessity of developing DT of production planning in automotive industry, depicting the guidelines for an effective implementation [9]. In the last years, the automotive industry massively applies DT considering wheel system and sub-systems for virtual sensing, homologation, and simulation of processes. In [10], Dal Borgo et al. developed a virtual sensor of the wheel angular position based on experimental measurements of linear displacement sensors. The methodology considers the model and measurement uncertainties due to sensor calibration, noise, and faults, but it is insensitive to the system topology variations, and it is not suited for design. In [11], a DT to diagnose aircraft tyre touchdown is developed using tyre geometry and working conditions parameters as yaw angle and tyre angular speed subject to normal distribution uncertainty. In [12], the uncertainty in fuel consumption during a driving cycle is estimated against variability in speed profiles, tyre parameters and rolling resistance coefficients, mitigating the necessity of physical experiments on test benches under physical constraints of component characterisation.

Moreover, researchers implemented DT for structural analysis and for Structural Health Monitoring (SHM) [13,14]. In [15], a real-time DT of electric vehicle motor is developed to prognose motor overheating. In [16,17], DTs of automotive braking systems are developed by coupling different modelling techniques for each subsystem (0-D electrical, 1-D hydraulic, and FE mechanical) estimating the wear of the brake pad. In [18], the flow forming process applied to automotive steel wheel has been completely developed by a FE model-based DT of the process, coupled, and validated by digital photogrammetry; the result shows that FE technique is relevant in process-related DT where real-time requirements are less strict, but simulation process is faster and cheaper than prototyping and experimental campaigns.

Numerical simulations are extensively employed in the automotive industry, encompassing various components, including the tyre. Accurate estimation of the wheel behaviour relies on understanding the loads exerted on it during operational conditions. However, wheel Original Equipment Manufacturers (OEMs) often lack sufficient knowledge and control over the tyre, introducing uncertainty into the design approach.

Different strategies have been analysed in this introduction, to understand advantages and limitations.

Tyre semi-empirical models such as MF-Tyre and MF-SWIFT find extensive usage in vehicle dynamics, Noise, Vibration, and Harshness (NVH), and tyre durability assessments [4]. Recently, in [19] a real-time vehicle dynamics model is developed, while in [20] a vibration suppression control strategy is developed and tested on a vehicle multibody model. In both cases, the models rely on Pacejka "Magic formula" MF-Tyre model for the estimation of exchanged contact forces.

The tyre semi-empirical models are not projected to study wheel flexibility which is negligible in the usual fields of application: MF-Tyre considers the wheel infinitely rigid [1]. Moreover, the vehicle dynamics frequency of interest range is $1 \div 10$ Hz, NVH-related tyre behaviour maximum frequency of interest is about $120 \div 140$ Hz, while the first natural frequency of conventional steel wheels exceeds 200 Hz (over 500 Hz for aluminium alloy wheels). Furthermore, semi-empirical models rely on equivalent structural characteristics linking the suspension to the ground and do not provide the necessary correlation between axle loads and the distribution of load induced by tyre deformation on the rim, making them unsuitable for calculating rim interface loads [4]. Coherently, the dominant software in the market for wheel simulation is semi-empirical model-based and tyre focused [21,22].

In 2017, Ballo et al. developed a semi-analytical model of pneumatic tyre specifically addressing the flexural contributions of the tyre sidewall and the calculation of the distribution of reaction forces amongst rim flanges, albeit limitations in accurately describing tyre-rim interactions that replicate test bench loading conditions for significant steering angles [23]. Eventually, tyre analytical models of vertical behaviour can be updated through the evaluation of systemic structural properties by experimental procedures [24].

Concurrently, Finite Element (FE) tyre models have been introduced by researchers as an alternative approach. The state-of-the-art has seen various improvements, incorporating solid, membrane/shell, and beam elements to enhance the description of anisotropic behaviour. During the 2000s, research efforts focused on enhancing the reliability of FE models by refining material characterization and the boundary conditions at the rim. The transition from axisymmetric formulations to three-dimensional (3-D) models utilizing 8-node and 20-node hexahedral elements enabled the study of contact patches and loading conditions beyond the plane [25–27]. Yang developed a 3-D FE tyre model using ABAQUS, with a focus on experimental characterization of material properties and image processing of tyre cross-sections to ensure accurate stress analysis on the tread inner liner during rolling conditions. This work highlighted the importance of having precise tyre cross-section data for reliable simulations [28]. Similarly, Baranowski et al. based their 3-D FE model on tyre cross-section microscopy and sidewall X-ray photography, further emphasizing the significance of high-quality data for accurate modelling [29].

In 2016, Shokouhfar et al. replaced the conventional hexahedral FE with multiple layer shell elements of equivalent properties. This substitution demonstrated the reliability of the obtained results in scenarios involving cornering, vertical load conditions, and modal behaviour [30]. More recently, Wan et al. conducted simulations on the fatigue life of a commercial vehicle wheel using biaxial fatigue tests. Their approach relied on a 3-D FE model, utilizing the Mooney-Rivlin hyper-elastic model to accurately depict the behaviour of the tyre rubber. During operation, the rim and the tyre were tied together [31]. In contrast, Santiccioli et al. employed the CDTire/3D tyre model to calculate the generalized forces on the wheel rim resulting from various loading conditions [32].

FE technique is also used by Bonisoli et al. for structural dynamics purposes on motorcycle field to track mode chassis mode shapes where a flexible wheel of linear 4-node shells is used [33]. Moreover, the methodology is useful in application where iterative design process must be fast, and it is necessary to identify the most critical component without expensive flexible multibody simulations [34]. It was demonstrated the necessity in considering the wheel flexibility in the identification of the most significant system mode shapes concurring in motorcycle handling [35].

Beyond the tyre modelling, also wheel require particular attention.

The automotive steel wheel i.e., the assembly obtained by press-fit of the disc and the rim components, is subject to residual stresses

and pre-stress. Since the wheel is the object of interest of this activity, these mechanisms as source of residual stresses are identified:

- Disc and rim forming and coining processes: which induce plastic deformation [36];
- Disc-rim interference fit [37–39];
- Disc-rim welding [36].

Instead, the following mechanisms are external stress causes, inducing pre-stresses:

- Disc hub bolt tightening [36–39];
- Tyre-rim axial/radial fitting (elastic);
- Tyre inflation pressure;
- Testing conditions.

In every analysed study, the complete characterization of residual stress and pre-stress is incomplete. The biaxial fatigue test of the wheels is presented in [36] does not consider the disc-rim fitting. Similarly, the determination of the service stress in a wheel due to vertical and horizontal loads, as well as the stamping production process, is discussed in [40]. However, even in this scenario, the comprehensive assessment of residual stresses is absent.

The tyre-rim fitting phenomenon is crucial in steel wheel pre-stress estimation. Initial efforts [41,42] were focused on indirectly estimating loading conditions through the utilization of diverse sensors for experimental measurements on the wheel. In years, direct [41] and indirect approaches [42] have been introduced for tyre-rim interface characterisation and stress recovery and indirect estimation of rim contact pressure.

Recently, the authors developed meta-models for the indirect estimation of interference fit in automotive steel wheels between the disc and the rim during the press-fit assembly process. In [37,38], the variability in structural properties as natural frequencies was correlated to geometrical and material uncertainties by a polynomial chaos expansion, and a first fatigue assessment based on FE model was performed and demonstrated being in line with the experimental fatigue life confidence levels. It was demonstrated the FE model is the proper tool to reduce experimental testing in industrial environment with minimal computational effort. In [39], the methodology was generalised to press-fit assemblies, formulating a training procedure which minimizes the experimental effort, and a fast in-line testing procedure. Nevertheless, the training is necessary and cannot be scaled to other similar components, limiting the usage of the methodology to industrialised components.

The integrated design process requires to iteratively develop prototypes which undergo experimental testing. In this process, the wheel is equipped with strain gauges at specific locations, and local strain is measured during the machine testing. These strain gauges are positioned near the sites where crack initiation has been identified in prior experimental tests [43,44]. Precise placement adjustments are made to prevent premature fatigue failure of the strain gauges during the trial. Importantly, these methodologies do not rely on tyre-specific knowledge but instead focus on the physical assembly of the tyre and wheel, which may not be available in the initial stages of the wheel design process. The application of strain gauges is non-destructive, and the obtained measurements can be directly compared with the strain distribution predicted by numerical models. Since strain gauges primarily provide localized strain information, patterns of strain gauge readings are used to enhance the spatial resolution.

Table 1
Comparison of wheel simulation methodologies.

Methodology	Rim forces	Flexible rim	Residual stresses	Radial test	Biaxial test
Semi-empirical models (MF-Tyre, MF-SWIFT) [4,19,20]	–	–	–	–	–
Semi-analytical model [23]	✓	–	–	no slip	–
cosin FTire/rim (FE) [21]	✓	✓	–	–	–
ITWM CDTire/3D [22]	✓	–	–	–	–
FE linear anisotropic [25–30]	✓	–	–	✓	–
FE hyper-elastic [31]	✓	✓	–	–	no OTM
FE + CDTire/3D [32]	✓	✓	–	–	no OTM
Full FE [36]	✓	✓	no press-fit no tyre fit	✓	–
Full FE [40]	–	✓	no press-fit no tyre fit	–	–
Experimental data based polynomial form [41,42]	✓	intrinsic	intrinsic	no slip	–
FE + CDTire/3D [37,38]	✓	✓	no forming no welding	✓	no OTM
Presented work	✓	✓	no forming no welding	✓	✓
Future work	✓	✓	no welding	✓	✓

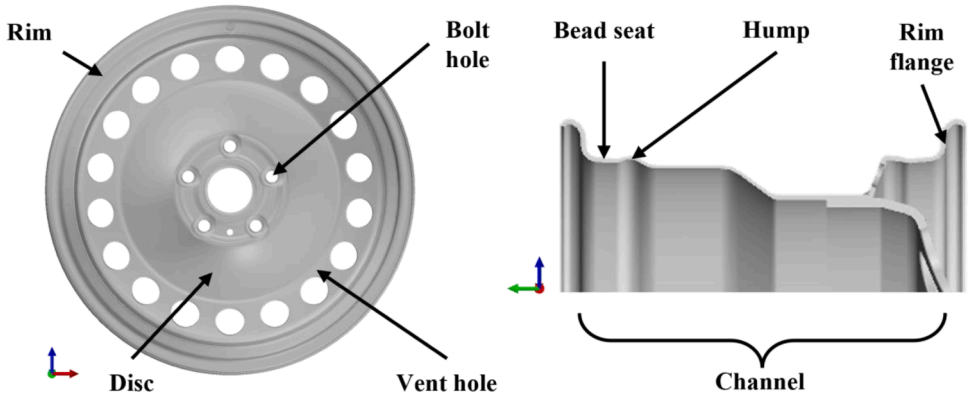

Fig. 1. Automotive steel wheel terminology.

Table 1 summarises the features of all the wheel behaviour simulation methodologies and their compared to the developed technique in this paper. The developed models by the authors in [37,38] were already capable to depict stress distribution in the wheel in different fatigue test scenarios. In our study we neglect the contributions of the forming processes, since the experimental mapping of the residual stresses was not available, and of the welding, since it was not applied to the studied sample wheel.

Nevertheless, limitations are present for biaxial fatigue tests since Overturning Moment (OTM) procedure was not simulated, making the model partial dependent from the experimental results during calibration.

The objective of the paper is to develop a feasible DT of the automotive wheel for the biaxial fatigue test-rig loading conditions with computation of consistent initial conditions through the simulation of the OTM procedure. The proposed DT is FE model-based and relies on the decoupled simulation of tyre behaviour under rigid rim hypothesis, and wheel behaviour under reaction forces computed by a propose rigid tyre-rim interface.

Currently, the OTM procedure is performed by biaxial fatigue test benches only, therefore, simulating the procedure makes the developed DT completely autonomous after geometrical and material properties of the wheel are supplied. Moreover, forming residual stresses will be implemented in the future works.

The paper is divided in four sections, supplying the terminology, describing the developed DT architecture, the proposed methodologies, and the validation process performed against an experimental industrial case study.

In Section 2, the necessary nomenclature and terminology are supplied.

In Section 3, the developed DT architecture is presented, depicting the main simulation steps, and the levels of communication through the different decoupled simulation environments.

In Section 4 the methodology is presented: the simulated OTM procedure, and the developed tyre-rim interface to adapt the tyre generalised reaction forces into lumped generalised forces on a FE wheel model are defined.

In Section 5 the industrial case is described, and the experimental and numerical tests are performed. The validation of the methodology is performed on camber angle related to a biaxial fatigue test loading program and on consequent stress analysis based on strain gauge measurements.

Finally, conclusions are dedicated to the discussion of results.

2. Terminology and nomenclature

In this section, the terminology related to the wheel and tyre, and the nomenclature of all quantities defined and adopted in the proposed methodology are presented. Fig. 1 shows the main components of the automotive steel wheel, or wheel, and the terminology

Fig. 2. Tyre terminology.

Table 2
Wheel behaviour and OTM procedure nomenclature.

Symbol	Definition	Unit
γ	Camber angle	[rad]
γ_e	Effective carcass camber angle	[rad]
γ_{tr}	Trial camber angle	[rad]
$\Delta\gamma$	Camber angle range limit threshold	[rad]
γ_{OTM}	Camber angle satisfying OTM condition	[rad]
h	Track-to-wheel centre vertical distance	[m]
r_l	Tyre loaded radius	[m]
$\overline{WP}$	Pneumatic scrub or carcass lateral deformation	[m]
y_C	TC wheel lateral displacement	[m]
$y_{C,0}$	TC wheel initial lateral displacement	[m]
$y_{C,curb}$	TC wheel lateral displacement at curb contact	[m]
z_C	TC wheel vertical displacement	[m]
$z_{C,0}$	TC wheel initial vertical displacement	[m]
F_{Y_C}	TC lateral force on wheel	[N]
F_{Z_C}	TC vertical force on wheel	[N]
M_{X_C}	Overturning moment	[Nm]
F_{Y_W}	TW lateral force on wheel	[N]
F_{Z_W}	TW vertical force on wheel	[N]
M_{X_W}	TW longitudinal moment at centre of contact patch	[Nm]
k_L	Tyre lateral stiffness	[N/m]

Table 3
Tyre-rim interface nomenclature.

Symbol	Definition	Unit
n_t	Number of nodes in tyre sidewall mesh	[-]
n_w	Number of nodes in rim flange	[-]
$\overline{BC}$	Tyre sidewall point of action bead distance	[m]
$\overline{CR}$	Minimal tyre sidewall-rim flange distance	[m]
δ	Tyre sidewall deflection	[m]
r_A	Nominal tyre radius	[m]
r_B	Rim channel half distance	[m]
r_C	Nominal tyre half width	[m]
θ	Rim Flange-hump line of action angle	[rad]
F_a	Rim axial reaction	[N]
F_r	Rim radial reaction	[N]
$F_{b,p}$	Tyre bead tension	[N]
$F_{b,r}$	Tyre bead-to-rim hump radial force	[N]
$F_{\delta,a}$	Tyre sidewall deformation axial force	[N]
$F_{\delta,r}$	Tyre sidewall deformation radial force	[N]
$F_{p,a}$	Tyre inflation pressure-to-rim flange axial force	[N]
$F_{p,r}$	Tyre inflation pressure-to-rim hump radial force	[N]
$\vec{F}_t$	Tyre sidewall force	[N]
$\vec{T}_t$	Tyre sidewall moment	[Nm]
$\vec{F}_w$	Rim flange force	[N]
$\vec{T}_w$	Rim flange moment	[Nm]
k_b	Tyre sidewall flexural stiffness	[N/m]
p	Inflation pressure	[N/m^2]

of the component regions approached in the next sections. Also, Fig. 2 presents all the tyre terminology used in the next tyre-rim interface section. Table 2 lists all the quantities used for the formulation of the OTM procedure used in the developed DT. In Table 2, the generalised forces acting on the rim flanges are represented in two different established reference frames [45]:

- TYDEX C-axis (TC) with origin of the axis fixed in the centre of the wheel, X_C axis is in the central plane of the wheel and parallel to the ground, Y_C and Z_C axes are inclined by camber angle;
- TYDEX W-axis (TW) with origin in the centre of tyre contact patch, X_W axis is in the central plane of the wheel and parallel to the ground, Z_W is normal to the ground.

Independently from operative conditions, Y_C, Z_C, Y_W and Z_W lay on the same plane orthogonal to the ground. Finally, Table 3 contains all the variables related to the tyre-rim interface model.

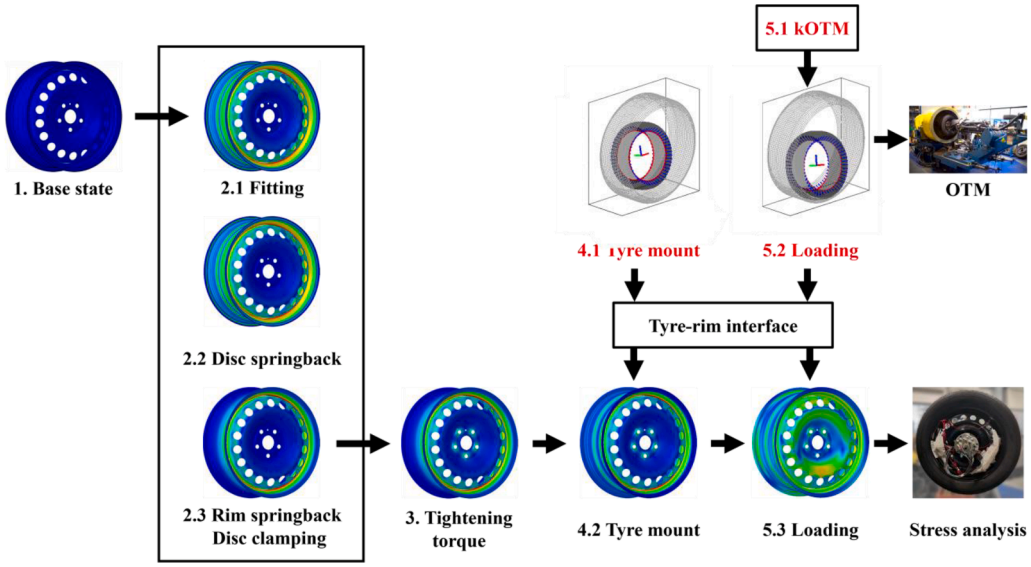

Fig. 3. DT architecture scheme.

3. Digital twin architecture

In this section, the adopted DT architecture is presented and discussed. The DT relies on a FE steel wheel model based on the results obtained in [46,47] and improved and detailed in [48]. It is an isotropic material, first order shell element-based FE model, introducing distinct stages of static analysis to also consider the residual stress and pre-stress induced during the assembling and mounting steps of the automotive steel wheel. The FE model ideally follows the manufacturing and mounting process, by finally applying the loading conditions.

The tyre and the wheel behaviours are simulated separately. The tyre behaviour is simulated in CDTire/3D under rigid wheel hypothesis. The reaction forces of the tyre simulation are then manipulated by the proposed tyre-rim rigid interface and applied to the FE wheel model in ABAQUS.

Fig. 3 shows the DT architecture scheme, with the significant simulation steps and estimation steps. Starting from left:

- The *Base state* represents the initial undeformed reference state of the wheel, where there is overclosure between the rim and disc. No residual stress or loads are induced by overclosure of the components to the geometry;
- *Fitting* stage involves resolving the overclosure between the rim and disc. The disc and rim flanges are clamped by boundary conditions (BCs) to the ground to simulate the press-fit process [39];
- *Disc springback* is the phase where the clamp BCs at the disc are removed, allowing for springback deformation;
- *Rim springback and Disc clamping* involve clamping the disc in its new position while removing the rim BCs. This step removes a portion of the elastic residual stress caused by the previous BCs;
- *Tightening torque* is applied by applying an equivalent nodal force to the annular regions of the bolt holes. Despite the tightening torque is applied after tyre mounting, this simulation step is anticipated to obtain a pre-stressed FE model with only parametric load to be applied; further details in [48];
- *Tyre mounting* is the phase where the pre-simulated CDTire/3D generalised reaction forces, including the contribution of inflation pressure, are imposed. The loads are manipulated using the developed rigid tyre-rim interface. This loading condition is simulated for a pre-simulation time of 0.5 s prior to the subsequent steps;
- *Loading* phase consists of a series of static analyses, where the computed generalised reaction forces from CDTire/3D for prescribed loading conditions and the imposed kinematics computed by the simulated OTM procedure are used as the load profile;
- *Tyre-rim interface* is the developed manipulation step where the tyre sidewalls external generalised reactions calculated by CDTire/3D simulation package are transferred to ABAQUS FE model to perform the remaining simulation steps;
- *kOTM* is the developed methodology to perform the calculation of kinematics parameters for simulation satisfying the physical OTM procedure requirements;
- *Stress analysis* and *OTM* are the two levels of experimental data evaluation.

To validate the developed DT, two different experimental to numerical comparisons are defined in the architecture. The first validation stage regards the kOTM procedure and requires the comparison with actual experimental OTM process on the biaxial test bench.

The second validation stage is focused on stress analysis on target locations on the steel wheel, comparing experimental stress

estimated by strain gauge measurements with calculated stresses on the wheel FE model. The validation process will be discussed in the Section 5 in detail.

4. Proposed methodology

In this section, the OTM procedure and the tyre-rim interface are developed. The proposed strategy consists of matching commercial Finite Differences (FD) physic based tyre model with customised FE wheel model. CDTire/3D simulation package is adopted to use the FD tyre model. The tyre model works under the hypothesis of interface with an infinitely rigid wheel, and it is subject to defined loading conditions and imposed kinematics characteristics. The kinematics characteristics are estimated with an iterative technique to obtain null overturning moment at the centre of tyre contact patch. The resulting tyre generalised external reactions are passed to a tyre-rim interface and then applied on a FE wheel model to perform stress analysis, and eventually fatigue life calculation. Sequentially, this section discusses:

- The procedure for the estimation of the imposed kinematics parameters to obtain null overturning moment for certain loading conditions;
- The developed tyre-rim interface to convert tyre generalised reaction forces in forces applied to the wheel.

4.1. Simulated overturning moment procedure

The biaxial test bench is an accelerated tyre contact simulator capable of dynamically applying both radial and lateral loads, with the ability to vary these loads throughout the testing process. Additionally, it can replicate acceleration and braking conditions within the test procedures.

The apparatus, depicted in Fig. 4 from the original patent and MTS 855 mutiaxial fatigue test bench [49,50], tests the wheel resistance to fatigue under accelerated and scheduled loading conditions. Furthermore, it serves as a valuable tool for the development of new products.

Additionally, it allows for the simultaneous testing of the vehicle's original brakes and hubs alongside the wheel. The drum presents two curbs which increase the maximum applicable lateral load during operation. The loading conditions are defined to bring in contact only the tyre thread with the drum. The test bench for fatigue assessment requires the application of a certain load program pattern, composed by a set of stationary loading conditions in terms of prescribed vertical load and lateral load.

Fig. 5 shows the generalised forces acting in stationary conditions on the tyre rolling on a straight surface subject to a combination of loads and, on the right, also to an imposed camber angle.

The wheel is subject to generalised forces which can be described in TC and TW reference frames [45]. It is possible to transform the generalised forces from TC to TW reference frame by using the following relationships:

$$\begin{Bmatrix} F_{Y_W} \\ F_{Z_W} \end{Bmatrix} = \begin{bmatrix} \cos\gamma & -\sin\gamma \\ \sin\gamma & \cos\gamma \end{bmatrix} \begin{Bmatrix} F_{Y_C} \\ F_{Z_C} \end{Bmatrix} \tag{1}$$

$$M_{X_W} = M_{X_C} - F_{Y_C}\, r_l \tag{2}$$

In which C and W subscripts refers to TC and TW reference frames, γ is the camber angle, and r_l is the tyre loaded radius. M_{X_C} is also named OTM [51,52].

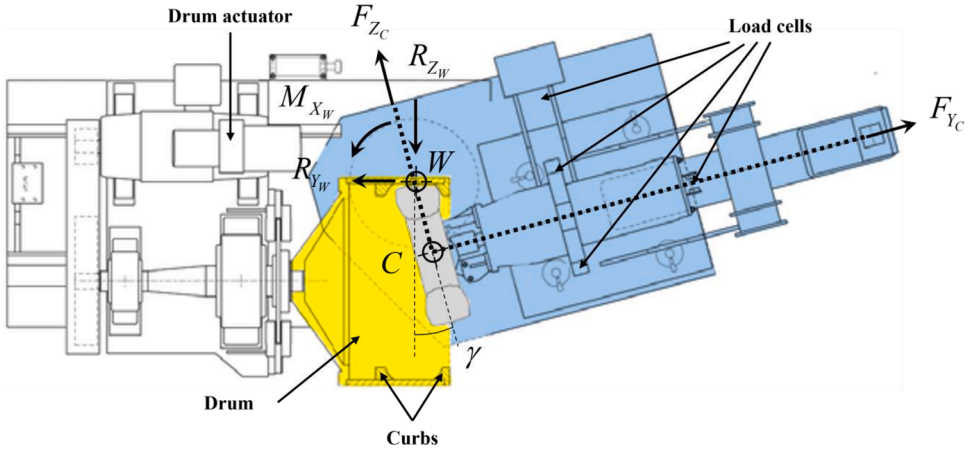

Fig. 4. Biaxial test bench. Cross-section of tyre-wheel assembly inside drum based on illustrations, free body diagram of tyre-wheel assembly [49,50].

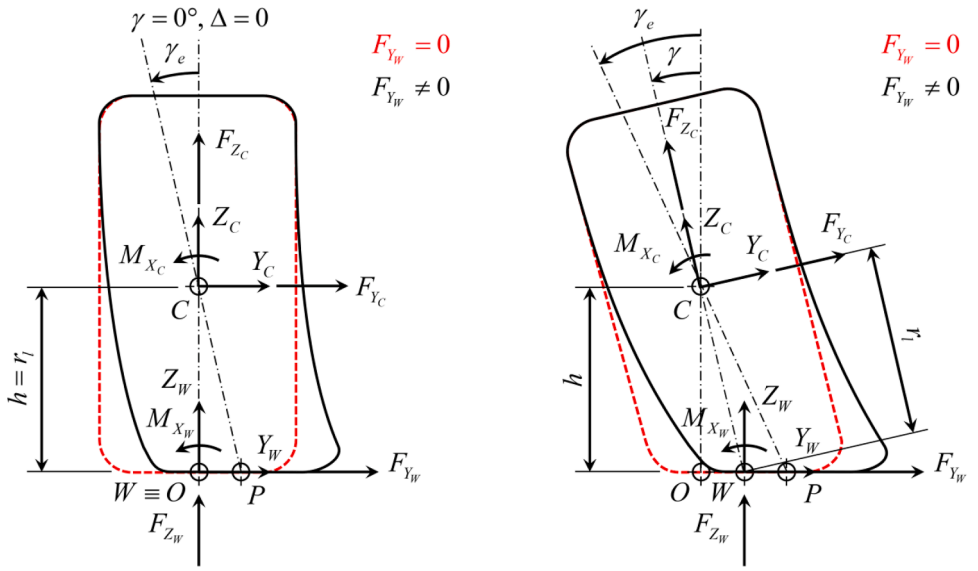

Fig. 5. Tyre behaviour in lateral plane: effect of lateral loads only (left), effects of lateral loads and camber angle γ (right).

Moreover, in the wheel lateral behaviour, it is valid the following trigonometric projection:

$$h = r_l \cos\gamma \tag{3}$$

where h is the track-to-wheel centre C vertical distance. From the application of loads, it is generated a carcass lateral deformation or pneumatic scrub $\overline{WP}$ which is the deviation of the deformed centre of the contact patch P from the undeformed one W. It is valid the following equation:

$$\overline{WP} = \frac{F_{Y_W}}{k_L} = \frac{M_{X_W}}{F_{Z_W}} \tag{4}$$

where k_L is the tyre lateral stiffness. The pneumatic scrub is, together with the generalised forces, used to calculate the effective carcass camber angle γ_e [53,54]:

$$\gamma_e = \tan^{-1}\left(\frac{\overline{WP} + r_l \sin\gamma}{h}\right) \tag{5}$$

The Eq. (5) is manipulated to back-calculate γ from quantities which can be easily calculated in CDTire/3D environment:

$$\gamma = \tan^{-1}\left(\frac{M_{X_W}}{F_{Z_W}\, h} - \tan\gamma_e\right) \tag{6}$$

To guarantee the correct functionality of the system under the prescribed loading conditions, it is necessary the OTM condition $M_{X_W} = 0$ is satisfied. The $M_{X_W} = 0$ condition is related to the working principle of the adopted biaxial fatigue test bench shown in Fig. 4. Since, the wheel actuator defining the camber angle is coaxial with the centre of contact patch, it is necessary to nullify the overturning moment at contact patch to avoid resistant torque on the actuator shaft. In high loading condition regimes, high resistant torque can damage the actuating system.

Under generic loading conditions, the contact patch may be over the curbs, therefore, the OTM condition can be written in a generalised starting from Eq. (2).

$$M_{X_W}(\gamma_{OTM}) = M_{X_C}(\gamma_{OTM}) - F_{Y_C}\, r_l(\gamma_{OTM}) = 0 \tag{7}$$

In order to satisfy the OTM condition in Eq. (7), a proper camber angle γ_{OTM} must be identified for prescribed F_{Y_C} and F_{Z_C}. For example, if lateral load F_{Y_C} is imposed null, the Eq. (7) is satisfied only if torque equilibrium around C is null, that is possible if we prescribe $\gamma_{OTM} = 0°$.

The CDTire model is adopted to calculate $M_{X_W}(\gamma)$ starting from prescribed loads. To perform the simulation, in the past Fraunhofer ITWM together with the authors, developed a CDTire/3D based environment to impose kinematic laws and loads on a pneumatic tyre interacting with a virtual drum for time domain simulations called CDTire/WTR [46]. The tyre is modelled under the hypothesis that the wheel and the drum deformations are orders of magnitude lower than the tyre one, hence both are assumed to be infinitely rigid. Beyond the geometrical characteristics of the tyre and the wheel, the developed environment allows to impose $y_{C,0}$, $\dot{y}_{C,0}$ and $z_{C,0}$, $\dot{z}_{C,0}$ wheel centre C displacements and speeds in TC reference frame, and wheel camber angles $\boldsymbol{\gamma} = [\gamma_1,\ \gamma_2,\ \gamma_3]$ to be reached at time instants

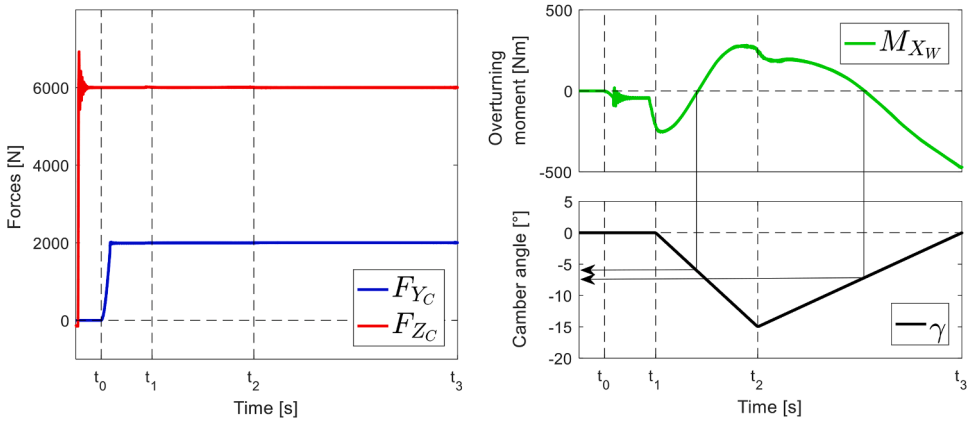

Fig. 6. Example of biaxial test manoeuvre in CDTire/WTR environment.

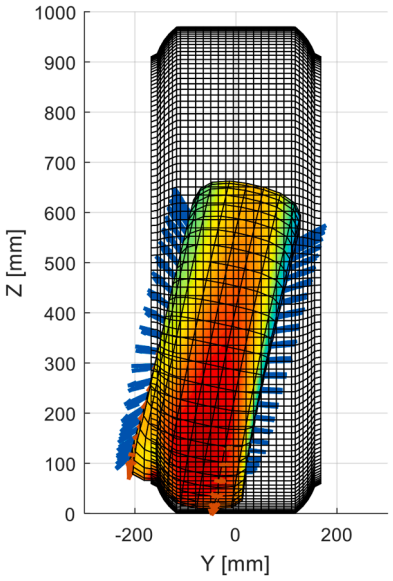

Fig. 7. Example of biaxial test manoeuvre in CDTire/3D environment: tyre tread-curb binding condition at t_2.

$\mathbf{t} = [t_1,\ t_2,\ t_3]$, respectively, with $t_1 < t_2 < t_3$. If two consecutives γ_i and $\gamma_{i+1}$are different, $\dot{\gamma}_{i,i+1} = (\gamma_{i+1} - \gamma_i)/(t_{i+1} - t_i) \neq 0$ defines a camber angle ramp law in that time period of the simulation. Further information on the implementation of the environment is available in [46,47].

Fig. 6 shows an example of biaxial manoeuvre with $F_{Y_C} = 2000$ N, $F_{Z_C} = 6000$ N, $\boldsymbol{\gamma} = [0,\ -15,\ 0]$ °, $\mathbf{t} = [1,\ 3,\ 7]$ s and defined $y_{C,0}$, $\dot{y}_{C,0}$ and $z_{C,0}$, $\dot{z}_{C,0}$ to better understand the procedure. The tyre initially approaches the curb with lateral constant speed $\dot{y}_{C,0}$ up to t_1, reaching a contact equilibrium at the wheel-to-curb lateral displacement $y_{C,curb}$.

Then M_{X_W} reduces as lateral curb reaction adds to lateral constant speed contribution. The tyre performs two triangular ramps of 2 and 4 s in which the maximum γ value $-15°$ is reached. The green curve describes the trend of M_{X_W} during γ change: it reaches the OTM condition twice with different γ values.

The manoeuvre is not reversible, since the tyre, through the wide camber angle ramps, reaches a condition in which the tyre tread is binded to the drum curb (Fig. 7). The non reversibility is visible from the M_{X_W} trend in the two γ ramps and from the jump at t_2. To overcome this nonlinearity, it is necessary to evaluate OTM condition in stationary equilibrium conditions, or for smaller γ ranges in which the behaviour can be linearised. The former is generally hard to perform since the wheel-to-curb lateral displacement $y_{C,curb}$ is not known a priori as depends, in statics, on γ. Also, increasing simulation time to perform quasi-static simulation is computationally expensive. The latter requires the definition of a smaller camber angle range $[\gamma_{tr,1},\ \gamma_{tr,2}]$ including γ_{OTM} for which an average wheel-to-curb lateral displacement $\overline{y}_{C,curb}$ is valid.

Therefore, it is proposed an iterative simulation approach mimicking the physical OTM procedure to choose a proper γ_{OTM}. Since the methodology relies on the iterative updating of kinematics parameters to satisfy OTM condition, we named the "kinematic OTM"

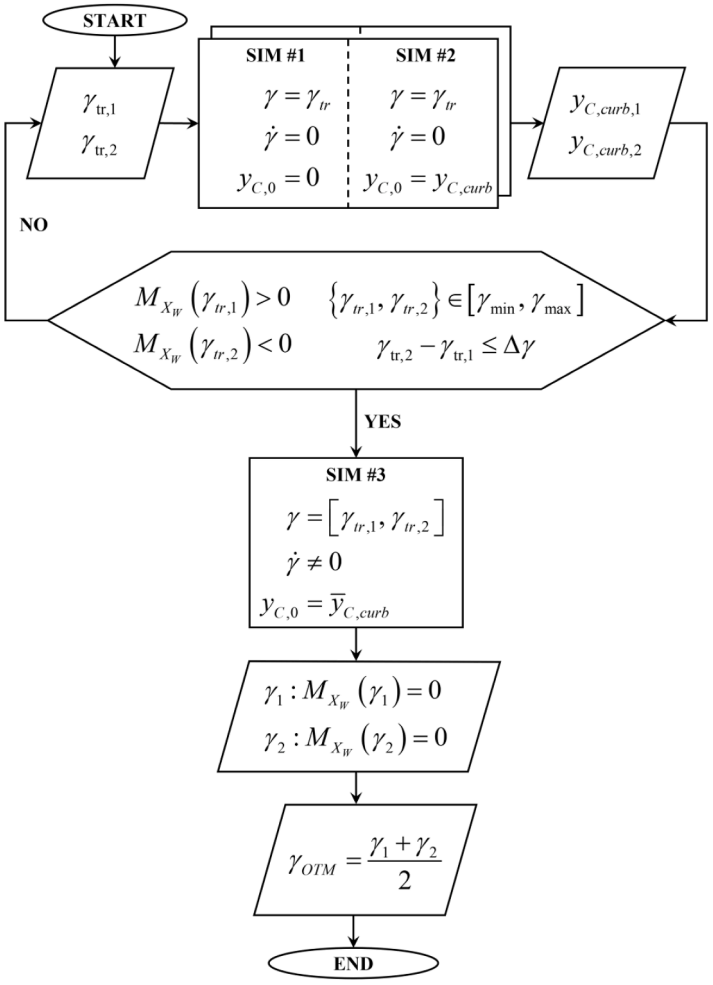

Fig. 8. Flowchart of simulated OTM procedure.

(kOTM).

The flowchart of the procedure is shown in Fig. 8, where two simulation stages are depicted: the first use the SIM#1 and SIM#2 simulation schemes, while the second one relies on the SIM#3 simulation scheme.

On the top of Fig. 8 the first simulation stage occurs: starting from a guess camber angle set $[\gamma_{tr,1},\ \gamma_{tr,2}]$, two sets of two simulations SIM#1 and SIM#2 are performed. The two SIM#1 simulations, with fixed camber angles $\gamma_{tr,1}$ and $\gamma_{tr,2}$, are used to identify a wheel-to-curb lateral displacement range $[y_{C,curb,1},\ y_{C,curb,2}]$. Two SIM#2 simulations verify the displacement range as kinematic parameters.

A validation stage verifies that four conditions are satisfied:

$$\{\gamma_{tr,1},\ \gamma_{tr,2}\} \in [\gamma_{\min},\ \gamma_{\max}] \tag{8}$$

$$\gamma_{\mathrm{tr},2} - \gamma_{\mathrm{tr},1} \le \Delta\gamma \tag{9}$$

$$\begin{aligned} M_{X_W}(\gamma_{tr,1}) &> 0 \\ M_{X_W}(\gamma_{tr,2}) &< 0 \end{aligned} \tag{10}$$

The Eq. (8) guarantees that the two γ candidates are inside the camber angle range of operability. The Eq. (9) guarantees the two γ candidates are close enough to consider linear and bijective the $M_{X_W}(\gamma)$ function. Finally, Eq. (10) must be guaranteed to ensure Eq. (7) can be satisfied in SIM#3. Perhaps, in SIM#3 the camber angle is linearly varied between $\gamma_{tr,1}$ and $\gamma_{tr,2}$, with $M_{X_W}(\gamma)$ bijectivity property it is ensured the existence of a $\gamma_{OTM} : M_{X_W}(\gamma_{OTM}) = 0$.

In the second simulation stage, γ_{OTM} is calculated. A single SIM#3 simulation is performed with constant $\dot{\gamma} \neq 0$ in the $[\gamma_{tr,1},\ \gamma_{tr,2}]$ range, also imposing $\bar{y}_{C,curb}$ averaging $y_{C,curb,1}$ and $y_{C,curb,2}$.

For each of the two SIM#3 simulations, γ_{tr} so that $M_{X_W}(\gamma_{tr}) = 0$ is identified and γ_{OTM} calculated as an average of γ_1 and γ_2.

The γ_{OTM} and $\bar{y}_{C,curb}$ are then usable for the complete simulation of the biaxial test in loading conditions: the kinematic parameters

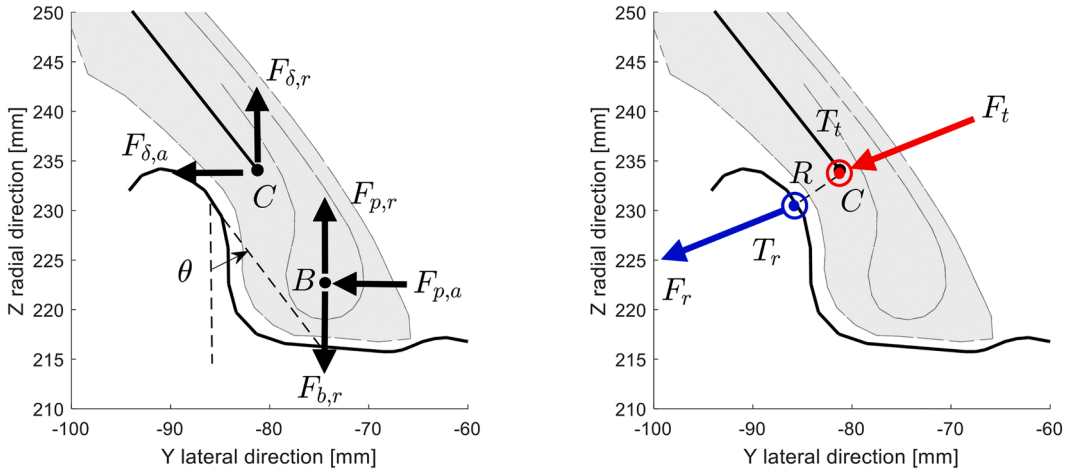

Fig. 9. In-plane interface: reference (left) [25], proposed rigid interface (right).

are used during the DT *Loading phase* in CDTire/3D as presented in Section 3 (see *Phase 5.2* in Fig. 3).

4.2. Tyre-rim interface

This subsection presents a newly introduced and developed model for addressing the interaction between the tyre and rim. The general forces of the tyre, obtained through CDTire/WTR, are assigned to the nearest node in the FE wheel model. CDTire/WTR assumes a fixed connection between the tyre and a rigid wheel, considering the tyre bead infill region and the bead itself. The tyre's general forces, including the effect of tyre inflation pressure [22], are applied without accounting for the possibility of tyre-rim contact loss.

The methodology description will primarily focus on hypotheses and definitions of force contributions, in comparison to existing approaches in the field.

In the proposed description, inspired by the recent work of Ballo et al. [23], the emphasis is placed solely on the reaction forces between the rim flange and the tyre sidewall. However, circumferential forces resulting from operational conditions are not explicitly discussed.

Fig. 9 illustrates the tyre-rim interaction forces in the in-plane view amongst flange and sidewall. These in-plane forces, distributed across the rim interface, are represented as concentrated contributions at the centre of the tyre bead and in the mid-space of the bead infill. Three main contributions are identified:

- The *inflation pressure* exerts a hydrostatic force per unit area p on the entire inner liner of the tyre. Its primary effect is to enhance the structural stiffness of the tyre by reducing the tension in the radial cords within the contact patch [55]. This force can be divided into concentrated contributions acting at the centre of the tyre bead B: a radial component denoted as $F_{p,r}$, which acts on the stiffer part of the tyre, and an axial component denoted as $F_{p,a}$, which is parallel to the rotation axis. As a result, a circumferential tension denoted as $F_{b,p}$arises in the bead to restrict the radial expansion of both the bead and sidewall.

$$F_{b,p} = \frac{p}{2}\sqrt{\left(r_C^2 - r_A^2\right)^2 - \left(r_C^2 - r_B^2\right)^2} \tag{11}$$

  where r_A represents the nominal tyre radius, r_B is half the inner rim channel width, and r_C is half the nominal tyre width [2].
- *Bead pretension* generated by the sidewall radial interference fit with the rim hump during tyre mounting. The effect is a radial component $F_{b,r}$ applied towards the rim and pointing the wheel rotation axis.
- *Tyre deformation* induced by loading conditions as a force per unit length which, for very stiff bead, can be approximated as a concentrated forces acting on sidewall node C, nearest to last tangent contact point between rim flange and sidewall external surface: radial load $F_{\delta,r}$ and an axial concentrated load $F_{\delta,a}$ are developed.

The normal-to-surface axial loading contributions result in a radial reaction relative to the inclined line of action. This line is inclined by an angle θ and extends from the point of maximum pressure on the rim hump to the last contact point on the rim flange fillet. In conclusion, the total radial and axial reactions F_r and F_a can be defined as follows:

$$\begin{aligned} F_a &= F_{p,a} + F_{\delta,a} \\ F_r &= \left(F_{p,r} - F_{b,r}\right) + F_{\delta,r} - F_{p,a}\tan\theta \end{aligned} \tag{12}$$

The $F_{p,r} - F_{b,r}$ quantity depends on bead stiffness [23], and tyre angular location: tyre locations opposite to contact patch are subject

Fig. 10. MTS 855 wheel biaxial fatigue test bench (courtesy of MW Italia S.r.l.).

Table 4
Tyre and automotive steel wheel specifications.

Characteristic	Property	Value
Tyre	Model [-]	215/55 R17
	p_{rel}, relative inflation pressure, [Pa]	$4.5 \bullet 10^5$
Wheel	Model [-]	6.5 J × 17 H2
	ET, offset [mm]	49
	n_b, number of bolt holes [-]	5
	T_n, tightening torque [Nm]	120
Disc material	t, thickness [mm]	4.2
	E, Young modulus [GPa]	210
	σ_Y, yield strength [MPa]	368
	σ_{UTS}, ultimate tensile strength [MPa]	610
Rim material	t, thickness [mm]	1.55÷2.4
	E, Young modulus [GPa]	203
	σ_Y, yield strength [MPa]	468
	σ_{UTS}, ultimate tensile strength [MPa]	522

to maximised $F_{p,r}$ as consequence of increment in tension of sidewall radial cords due to inflation pressure effect.

The proposed rigid interface considers the overall cross-sectional reaction contributions. To address the lack of knowledge about the wheel, additional assumptions are made in CDTire/WTR. Fig. 9 (right) serves as a reference sketch for illustrating the generalised forces at the tyre-rim interface:

- In each rim flange radial section, the tyre sidewall deformation is negligible;
- the bead is considered infinitely rigid in relation to flexural bead infill behaviour in the cross-sections. As a result, $F_{b,r}$, $F_{p,r}$, B and C points of actions can be considered uncoupled, and the point of action of $F_{p,a}$ is C;
- there is not loss of contact between tyre and the rim in C;
- the sidewall is fixed in C, hence a reaction torque T_t is developed at C.

The proposed rigid interface integrates the previous hypotheses to apply loads:

- the rim is stiff and loading conditions induce small displacements;
- since the sidewall is assumed to be infinitely rigid, keeping the distance $\overline{CR}$ fixed a threshold under in-line load;
- the distance $\overline{CR}$ is considered negligible, so it does not contribute to generating a torque arm.

The generalised reaction forces at C are defined by Eq. (13), where is $(\vec{i},\ \vec{j},\ \vec{k})$ the cross-sectional reference frame, k_b is the unknown sidewall flexural equivalent stiffness, and δ is the sidewall deflection with respect to C. Under the proposed assumptions and assuming an equal number of annular sections in the tyre mesh n_t and the wheel n_w i.e., the number of available mesh nodes in the FE

Table 5
ZWARP fatigue test load cases.

Load case	F_{Z_C} [N]	F_{Y_C} [N]	Load case	F_{Z_C} [N]	F_{Y_C} [N]
1	16104	−5086	12	12361	4309
2	4238	−1695	13	16104	5086
3	10171	−1695	14	10171	5227
4	5792	−1413	15	8829	5651
5	16104	0	16	10,736	7063
6	7628	0	17	15257	7134
7	6357	283	18	13279	7134
8	10171	1695	19	12714	8476
9	6498	1695	20	14126	8970
10	7063	2825	21	16881	9041
11	8970	4238	22	20623	10311

model in the circumferential direction, the generalised reaction forces are applied from the tyre nodes to the rim flange nodes as shown:

$$\begin{aligned}\vec{F}_t &= \left(F_{p,a} + F_{\delta,a}\right)\vec{j} + \left(F_{\delta,r} - F_{p,a}\tan\theta\right)\vec{k} \\ \vec{T}_t &= \left(k_b \delta \overline{BC}\right)\vec{i}\end{aligned} \tag{13}$$

$$\begin{aligned}\vec{F}_w &= \vec{F}_t \\ \vec{T}_w &= \vec{T}_t\end{aligned} \tag{14}$$

In the typical application case $n_t < n_w$, the concentrated generalised force fields ($\vec{\mathbf{F}}_t$ and $\vec{\mathbf{T}}_t$) at n_t locations are interpolated by distributing them circumferentially onto the nearest rim nodes using the λPCH technique [48]. The resulting concentrated generalised reaction fields ($\vec{\mathbf{F}}_w$ and $\vec{\mathbf{T}}_w$) at n_w are then scaled by the scale factor n_t/n_w. This approach converges to a distributed loading condition when $n_w \to \infty$.

5. Industrial case study

The proposed industrial case study has been developed at MW Italia S.r.l., which supplied the facilities and the samples for the experimental activities. The experimental data for the comparison is obtained from a campaign with an MTS 855 biaxial test bench (see Fig. 10) in C configuration [7,49] and the MTS OTM procedure provided with the machine control system. The tests are performed on a 6.5 J × 17 H2 automotive steel wheel mounting a 215/55 R17 tyre.

In Table 4 the specifications of the automotive steel wheel and the selected tyre for the tests are listed. For the first validation stage, the tests are performed following ZWARP fatigue scheme [49] and PV-5608 load program.

Table 6
OTM procedure computational cost analysis.

Load case	OTM procedure			FE model
	Number of iterations [-]	Iteration time [s]	Total time [s]	Solution time [s]
1	56	83	415	838
2	105	84	756	693
3	72	74	444	698
4	109	74	740	674
5*	1	72	72	721
6*	1	74	74	722
7*	1	71	71	703
8**	1	74	74	751
9	35	72	216	795
10	133	71	852	779
11	51	73	365	884
12	27	74	222	824
13**	1	83	83	826
14	46	74	296	763
15	120	73	730	799
16	73	75	525	850
17	176	74	1110	814
18	25	74	222	794
19	61	76	456	829
20	77	76	532	836
21	158	71	994	910
22	6	72	72	1083

5.1. Overturning moment procedure

To execute the whole load program, a total of 117 repetitions of a 32-step sequence are required. Each step is then repeated for a specified number of revolutions at a predetermined angular speed of 42.94 rad/s. The 32-step sequence consists of a not-sorted, with repetitions, sequence of a predefined set of 22 unique load cases, as listed in Table 5, with defined radial and lateral loads.

These load cases are applied on the MTS test bench following the completion of the experimental OTM process for each case, to identify γ_{OTM} per each load case.

In experimental OTM, lateral load F_{Y_C} is applied while γ is modified in a compatibility range. The test bench measures M_{X_C} and verifies to occurrence of the following equality based on Eq. (2):

$$M_{X_C} = F_{Y_C}\, r_l \tag{15}$$

The test bench executes a linear "ramp up-ramp down" manoeuvre in which γ is slowly increased in time. During the OTM process, the Eq. (15) is satisfied twice: the operative γ_{OTM} for the fatigue test is obtained by averaging γ measured at the two intersections. The final biaxial test will occur at forced γ_{OTM} and prescribed lateral and radial loads. The experimental and numerical OTM procedures are applied on all the load cases in Table 5.

The experimental OTM requires two camber angle ramps of 30 s each for each load case. Instead, kOTM is implemented in Matlab® and performed imposing $\mathbf{t} = [2,\ 6,\ 10]$ s and $\Delta\gamma = 2°$

The analysis is performed in parallel on two workstations. The OTM procedure is performed on a Dell Inspiron 15 7510 laptop, with 11th Gen Intel(R) Core(TM) i7–11800H @ 2.30 GHz processor, 16 GB of RAM. The OTM procedure is implemented using Matlab 2023a Parallel Computing Toolbox with 16 workers and parallel fmincon(γ,y_C) function.

The wheel FE model simulations are performed on a custom fixed workstation with AMD Ryzen 9 3950 × 16-Core processor (32 logical CPUs) 3.5 GHz processor, 32 GB of RAM. The FE model is developed and solved in Abaqus 6.20 with 14 parallel workers.

The wheel FE model steps from "Base state" to "Tightening torque" are simulated once. The simulation lasts 246 s. All the other load cases are simulated by 104 batch static analysis steps restarting from the previous initial result.

Table 6 lists the characteristics of each load case simulation, in which simulation time breakdown is described. For the OTM procedure the following details are supplied: the number of fmincon() iterations to solution; the iteration time, which is the time required by CDTire/WTR environment to perform the prescribed manoeuvre; the total time considering parallelised fmincon() solution.

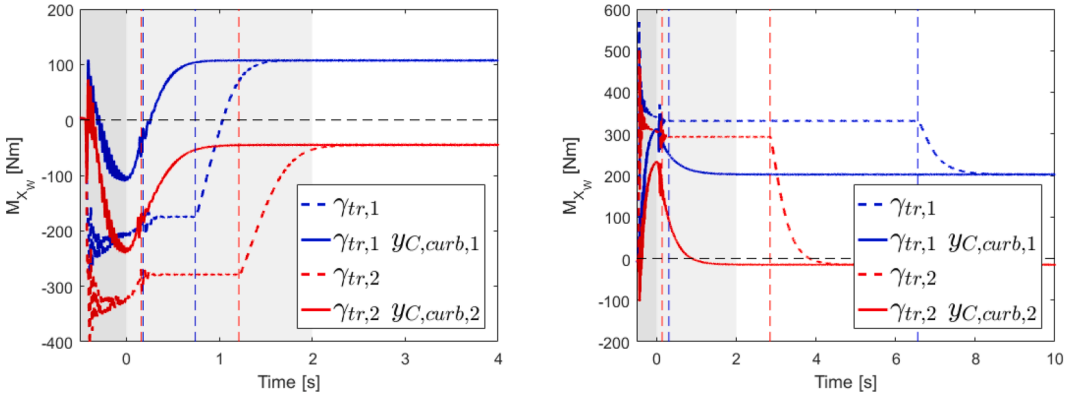

Fig. 11. $y_{C,curb}$ range calculation: load cases #3 (left) and #10 (right).

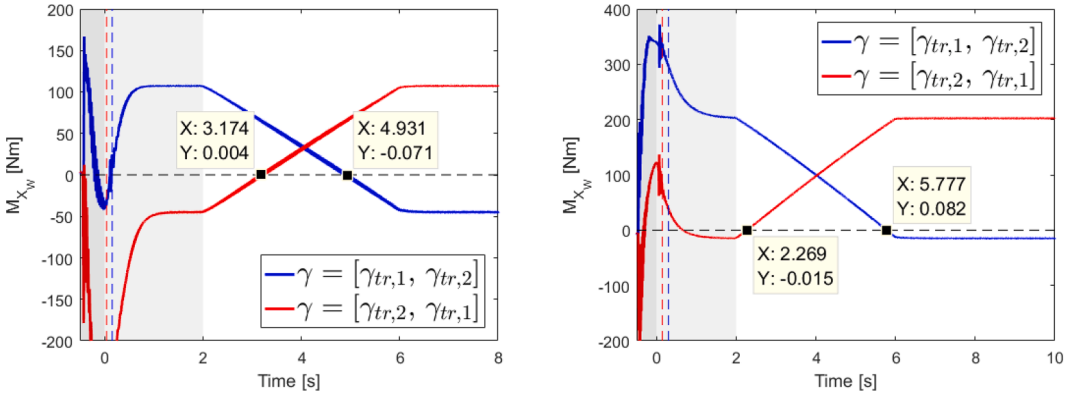

Fig. 12. Verification of OTM condition on $M_{x,W}$: load cases #3 (left) and #10 (right).

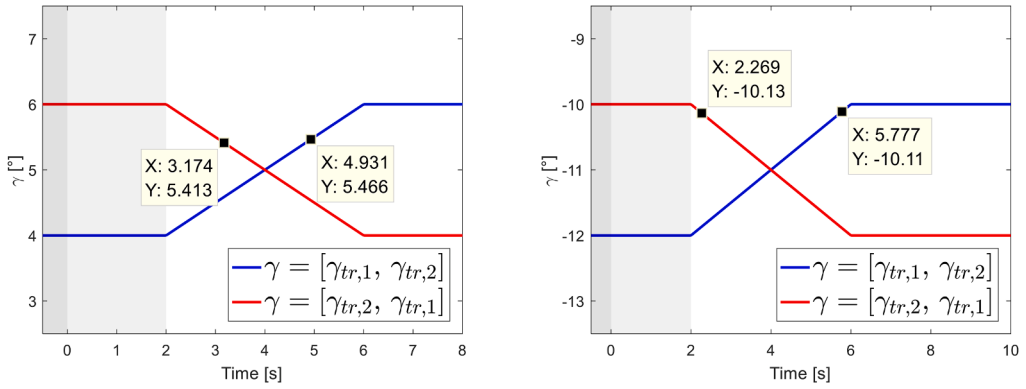

Fig. 13. γ_1 and γ_2 evaluation: load cases #3 (left) and #10 (right).

For FE model, the solution time of the "Tyre mount" and "Loading condition" steps is considered.

Particularly, Table 6 shows special treatments for "*" load cases, in which OTM procedure is not necessary, and direct CDTire/WTR solution is used. Similarly, "**" load cases are not subject to OTM procedure since the loading conditions are identical in magnitude to other loading conditions. Specifically, load case #1 is similar to #13, and load case #3 is similar to #8.

The overall OTM procedure for load cases lasts 155 min, while FE model 293 min.

The DT prediction is compatible with the experimental test timing. In fact, by considering the experimental setup times, the physical OTM procedure and manufacturing process times, the physical counterpart activity lasts 8 h.

Moreover, the obtained DT results can be directly used for fatigue analysis, while the accelerated biaxial fatigue test usually lasts days. The usage of decoupled simulation environments allows to drastically reduce computational complexity and simulation times, obtaining results even before the conclusion of the effective experimental test.

In Figs. 11–13 are shown the most significant quantities computed through kOTM procedure for load cases #3 and #10 to demonstrate the functionality of the methodology.

In Fig. 11 are shown the results of the ranging iterative process i.e., SIM #1 and SIM #2 simulations. In the graph it is shown a detail of M_{X_W} in the first 4 s of simulation. The blue lines refer to the $\gamma_{tr,1}$ behaviours, while the red ones to $\gamma_{tr,2}$; dashed lines are the simulations with $y_{C,0} = 0$, while full lines are the simulations with identified initial kinematic condition $y_{C,curb}$. The greyed regions are the pre-simulation steps, in which loading conditions are not applied, and initialisation step, in which starting γ, $\dot{\gamma}$ are applied. It is possible to notice the difference in system response due to the correction in lateral initial condition: in the corrected simulations the tyre reaches curb contact at the beginning of initialisation step around 0.2 s; the remaining simulation is a short transient to stationary $M_{x,W}$ value, which is, for each couple of $[\gamma_{tr,1}, \gamma_{tr,2}]$, over and below OTM condition $M_{X_W} = 0$. Load case #3 differs from #10 in the sign of expected γ_{OTM}: this is explained by the opposite saturation direction of $M_{x,W}$ in the two scenarios.

Fig. 12 shows the M_{X_W} result of SIM #3 simulations based on the imposed kinematic parameters evaluated in the previous part of the procedure, with the computed $\bar{y}_{C,curb}$: the blue lines describe the $[\gamma_{tr,1}, \gamma_{tr,2}]$ kinematic law simulation, while the red ones the opposite $[\gamma_{tr,2}, \gamma_{tr,1}]$ ones. As expected from Fig. 11, both the simulations trespass the OTM condition. The cursors indicate the abscissa values to be read in γ diagrams when OTM condition is satisfied.

Fig. 13 lists the γ diagrams in which cursors are placed where OTM condition is satisfied. As can be seen from the ordinate values, γ_1, γ_2 are almost identical, indicating the system behaviour is linearizable in the neighbourhood of the imposed kinematic condition.

Finally, Fig. 14 shows the comparison between experimentally and numerically evaluated γ_{OTM} for all the proposed 22 load cases. The DT developed methodology shows precise estimation of the operative camber angle with a maximum absolute relative error of 4.93% at load case #1.

The developed iterative methodology is compliant with experimental results and exploits the versatility of the CDTire/WTR environment to find operative kinematic conditions with an optimised and computationally inexpensive procedure.

5.2. Stress analysis

In this subsection, the second validation stage is discussed.

To assess the performance of the developed DT, an experimental campaign is conducted using a biaxial test load program that has been previously validated. This campaign involves measuring the strain variation at specific locations on the wheel using strain gauges. By combining the strain gauge test method with the biaxial machine, a comprehensive understanding of the stress distribution across the wheel during a load case is obtained.

The primary goal of this study is to evaluate the effectiveness of the DT in accurately describing the stress field throughout the entire steel wheel. Special attention is given to the zones of the tyre-rim interface, specifically the rim flanges. Deformations of the flange under biaxial loading conditions will be assessed by measuring strain using strategically placed strain gauges. along the circumferential and axial directions on both the inner and outer surfaces.

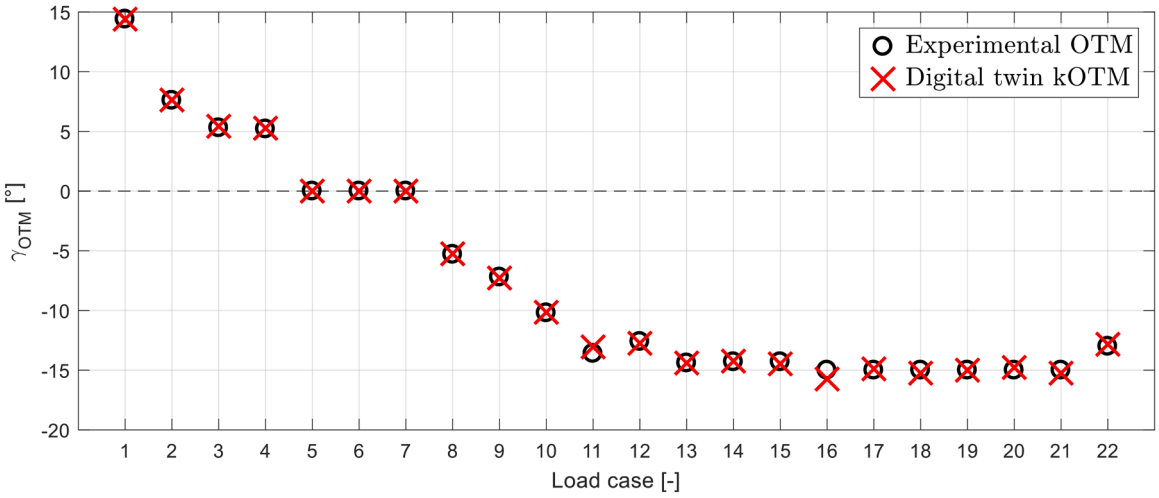

Fig. 14. γ_{OTM} comparison between experimental and kOTM procedure results.

The strain gauges are precisely placed on the wheel using a modified MoGeSeC algorithm [56]. The approach of selecting strain gauge positions based on strain-geometrical criteria enables the identification of key nodes for strain measurements. This approach primarily focuses on selecting appropriate data to represent direct stresses and effectively dividing the geometric domain. In the case of a steel wheel subjected to various loading conditions, a modified approach is employed for placing strain gauges. As a result, a map of six significant strain gauge locations is generated, with the approach also determining the orientation and application surface for each gauge.

Within Fig. 15, the arrangement of the strain gauges on the 6.5 J × 17 H2 wheel is depicted. The left side illustrates the angular positions of the strain gauges, while the right side specifies the exact locations of application. The right side highlights the point of application and the corresponding surface through a colour code i.e., the inner surface is represented by blue, while the outer surface is represented by red. Channels R1 to R3 correspond to the outer flange, whereas channels R4 to R6 relate to the inner flange. Channels R3 and R6 are mounted on the outer surface, which is a critical mounting point that may meet the tyre sidewall.

On the sample wheel (Fig. 16), six KYOWA KF-GS-1-350-C1-11 strain gauges were installed following the designated positions illustrated in Fig. 15. The application of strain gauges on the rim involved different techniques: strain gauges R1, R2, R4, and R5 were affixed using a cyanoacrylate adhesive on the appropriately sanded region, while R3 and R6 were also coated by a protective compound (AK-22 agent prescribed by the strain gauge producer). The presence of pre-conditioning and thermal drift correction electrical circuit could not be observed due to the covering paper packing tape and black insulating tape. To facilitate comparison with numerical results, a decision was made to reduce the number of load case repetitions typically conducted in fatigue tests.

Instead, a brief time history was recorded for each load case, but at a lower angular speed. The MTS test bench was manually operated to gradually increase the loads and camber angle until the desired test conditions were achieved. Experimentally, the strain time histories are acquired by a Rainer Thomas Messtechnik W8 universal telemetry wheel. The system allows a sampling interval of 637.5 μs. The numerical campaign is performed by using CDTire/WTR for the tyre behaviour simulations, LUPOS environment for model preparation and parametric application of loads [57], and ABAQUS for the steel wheel FE model and step-based simulation described in Section 4. Using the initial tyre orientation, a whole wheel revolution is simulated in ABAQUS as a set of quasi-static consecutive simulations. The stress histories in this study were derived from approximate average positions within the FE model. The numerical results were obtained from the stress fields in the ABAQUS output database, specifically at nodes. The stress values were averaged at 75% along with adjacent elements to simulate the averaging effect of strain gauges, considering the dimensionality of the measurements.

During the stress analysis, the final stress field was determined by comparing the loaded condition with the stress field obtained from the *Tyre mount* step. The *Tyre mount* step considered all the residual stresses resulting from fitting, clamping, tightening, and mounting processes. The difference between these two stress fields provided the comprehensive stress information for further analysis. Finally, the experimental strain campaign is compared with numerical results.

In Figs. 17 and 18, the comparisons of the mean stress and alternate stress of each location are shown. On abscissa, there are the numbered load cases, while stress components on the ordinates. Black markers are experimentally measured stresses, red markers are the DT outputs, and blue markers are relative percentual errors $100 \cdot |DT - \exp|/\exp$.

In Fig. 17, can be observed an overall good correspondence with local issues:

- at R1 and R4, i.e., radial direction on bead seat, the experimental trend is qualitatively captured by the DT. The R1 behaviour is overestimated at external bead seat up to 150 % even though the mean stress is small and maximum variation is about 10 MPa, hence the local stress condition is consistent. The R4 behaviour instead is critically underestimated up to −100 % up to 30 MPa of difference at internal bead seat for high lateral load conditions. This scattering in the DT estimation is mainly due to rigid tyre-rim interface working principle, which does not introduce equivalent loads on the bead seat regions;

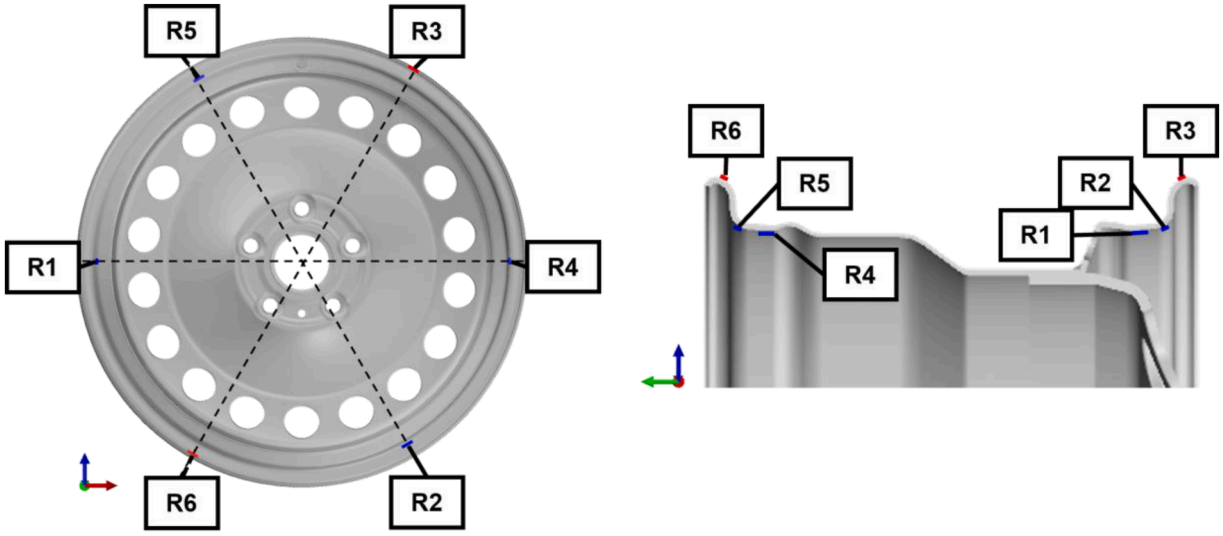

Fig. 15. Orientation of strain gauges: XZ plane (left) and cross-section (right).

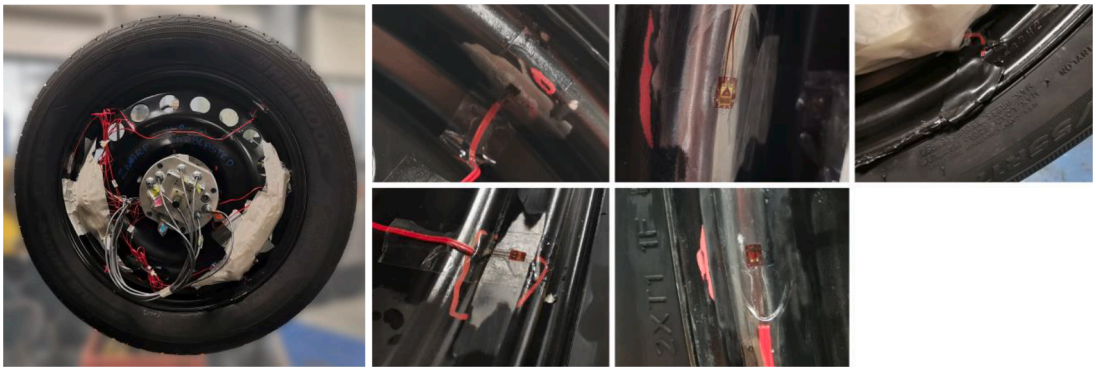

Fig. 16. Experimental setup on MTS 855 biaxial fatigue test bench.

- at R2 and R5 i.e., in the circumferential direction on the rim flange corners, the comparison is satisfactory; on R2 external rim flange, the mean stress is overestimated high F_{Z_c} load cases, while on R5 internal rim flange, the DT mean stress is generally underestimated for positive values of experimental mean stress;
- at R3 and R6 i.e., in the circumferential direction on the upper rim flange regions, the comparison is discrete; the two diagrams are greyed out from a certain load case, since the strain gauge connections failed during the experimental campaign; on R3 external rim flange region, the underestimation increases, up to wire connection failure, but with good correlation.

The comparison shows quantitative correspondence amongst the regions of application of concentrated loads by the tyre-rim interface i.e., R2, R3, and R5, while R1 and R6 are qualitatively estimated but suffer the lack of a proper loading application on the bead seat regions.

In Fig. 18, it is shown the comparison of the alternate stress of each location, with good correspondence:

- at R1 and R4, the alternate stress is generally overestimated up to 600 % for smallest experimental alternate stresses; on the inner bead seat the overestimation is only present for high F_{Y_c}/F_{Z_c} loading conditions up to 120 %. Similarly to previous considerations for Fig. 17, the overestimation is mainly caused by the tyre-rim interface, which does not depict the tyre bead filler flexibility;
- at R2 and R4, the comparison is almost perfect, significant underestimation up to −50% occurs on R5 inner rim flange, which is higher for lower alternate stress values;
- at R3 and R6, the comparison is optimal; R3 correspondence is very good until load case #8, from which underestimation occurs until failure of the wire connection.

Generally, the overestimation is proportional to the experimental amplitude i.e., larger relative percentual errors are obtained for smaller stress values; therefore, the phenomenon is linked to the overestimation of the sidewall stiffness in the rigid interface methodology.

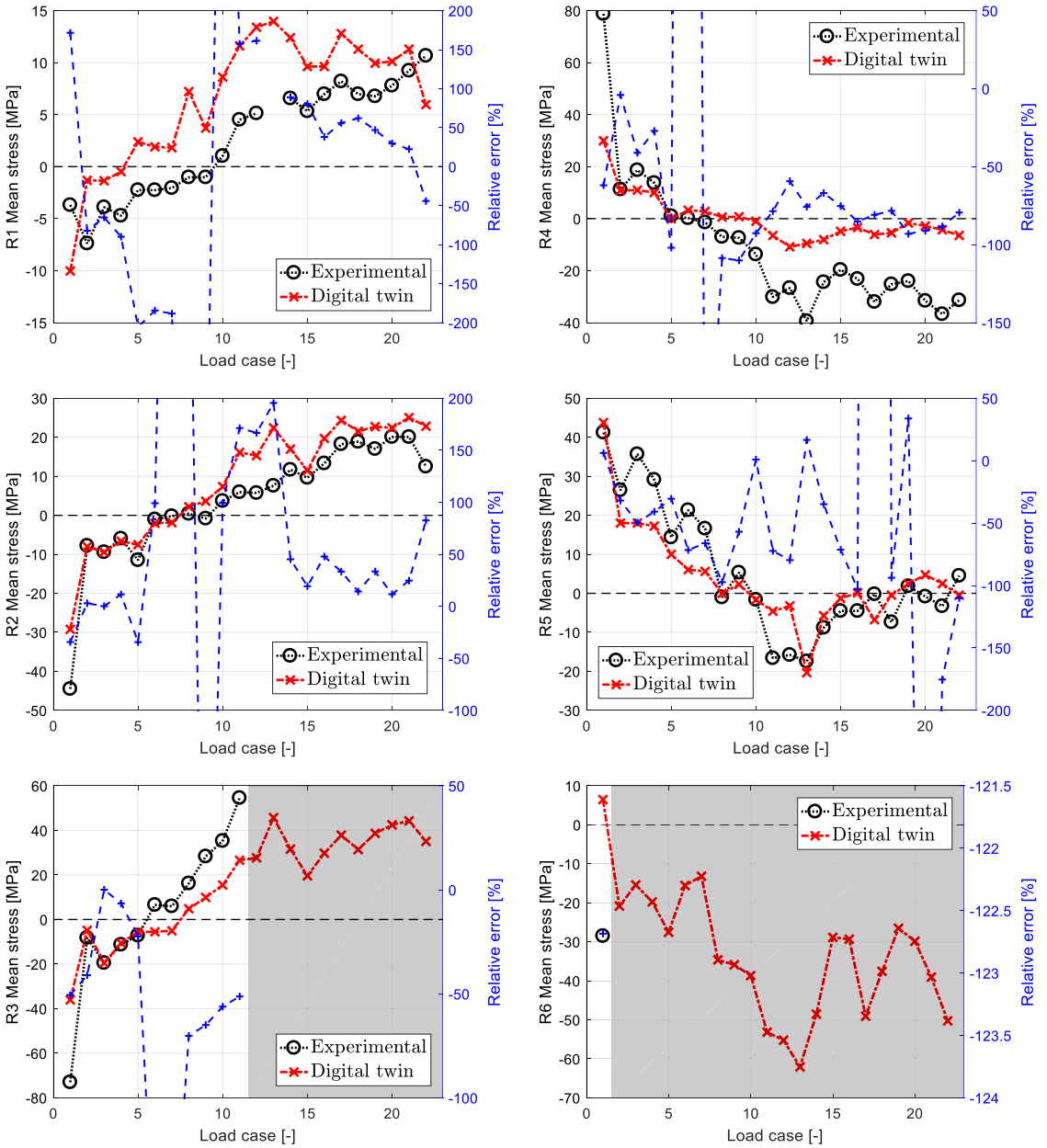

Fig. 17. Mean stresses related to experimental strain gauge measurements.

The methodology employed in this study yields consistent and reproducible results that are proportional to different loading conditions. While the magnitude of the maximum alternate stress is influenced by the applied load, the overall stress gradient across the geometry remains consistent. This suggests that the strain gauge locations can be standardized across different wheels.

In all cases, three strain gauges are used to monitor both flanges, and their performance is consistent. The chosen number of strain gauges is optimized to capture the alternate stress gradient accurately. Investigating the stress distribution across the entire cross-section helps explain the difficulty in identifying strain gauges that specifically measure radial alternate stress. This is because there is no significant gradient of radial alternate stress across the geometry.

As can be observed in Figs. 17 and 18, a systematic difference occurs in comparisons on internal and external rim flanges. This behaviour is strongly influenced by the different rim material distribution. For instance, the cross-section of the inner flange acts as a cantilever beam, bearing higher stress on the channel. On the other hand, the outer flange arm to disc is shorter, resulting in a stiffer support structure. Nevertheless, the CDTire/3D tyre model cannot capture this difference in rim flexibility since wheel is considered infinitely rigid. The R2 and R5 comparisons show the residual stress related to interference fit between rim and disc is correctly depicted.

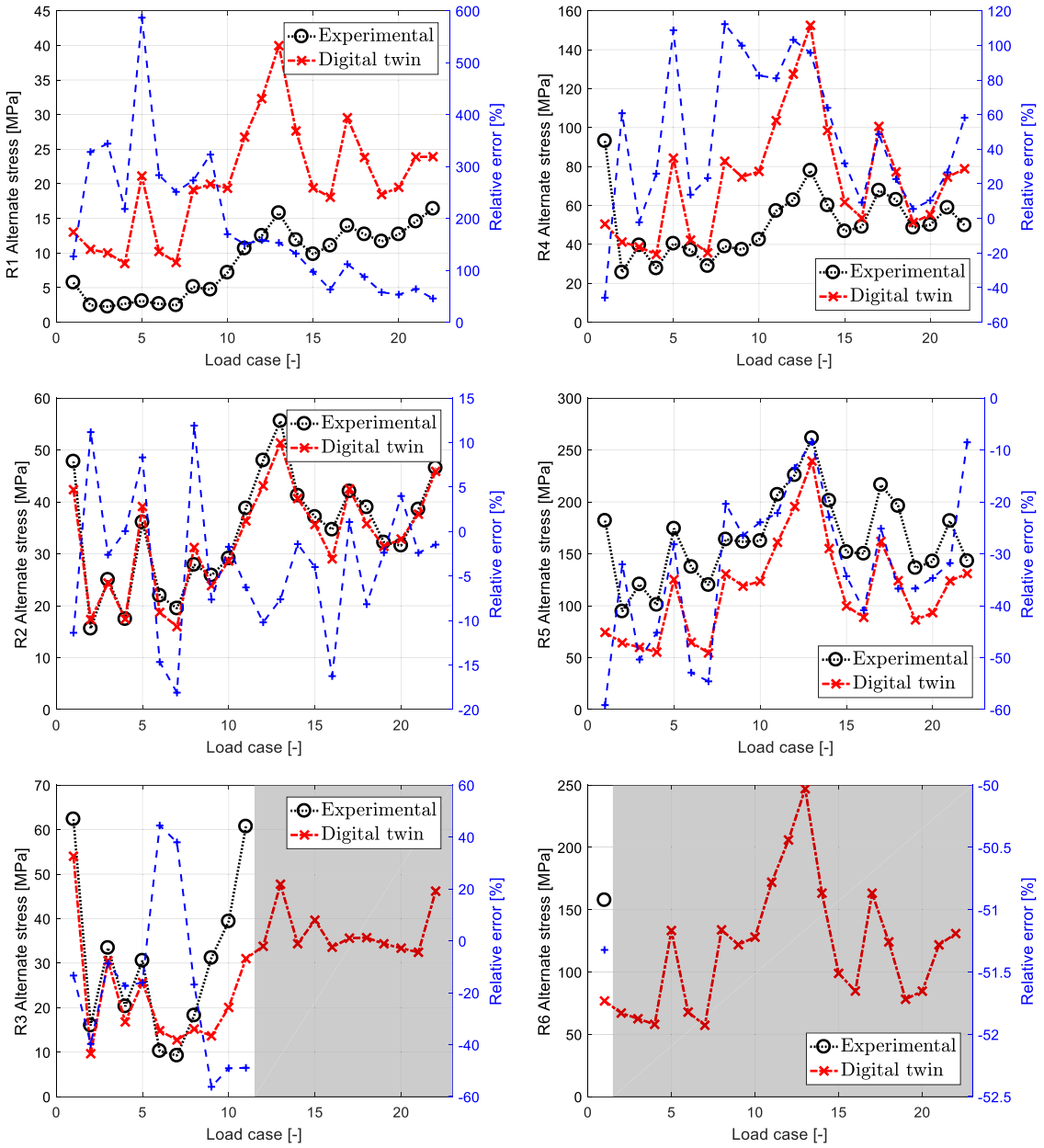

Fig. 18. Alternate stresses related to experimental strain gauge measurements.

In conclusion, the developed DT is reliable in low regime loading conditions, but sometimes alternate stress is far from expected experimental result.

6. Conclusions

In this paper, a DT of automotive steel wheel subject to assessment conditions is developed, discussed, and validated by comparison with experimental OTM results and strain gauge measurements.

It is proposed a novel DT which couples consolidated commercial software environments, ABAQUS and CDTire/3D, by an innovative tyre-rim rigid interface which considers the contribution of loading conditions, inflation pressure and bead pretension. A novel iterative procedure simulates the OTM procedure calculation, performed on wheel biaxial fatigue test benches.

These characteristics make the developed DT versatile against different sign camber angle loading conditions, to high regime loads, in anomalous contact patch conditions with tyre thread locally in contact with the curb, and capable to correctly describe the stress field amongst the whole wheel.

The developed kOTM is shown to be extremely effective in the estimation of the operative camber angle with small relative error compliant with the engineering application.

The tyre-rim rigid interface is capable of correctly describe the overall flange stress field, but it is limited in depicting the flange pressure distribution. It is suitable for the assessment conditions of the disc but lacks in correctly loading the flange. The main flaw is the impossibility to recover an index of contact pressure occurring at the flange.

In the future, the tyre-rim interface will be improved by allowing a flange pressure distribution not imposed in its physical model, which implies the passage to a stiff interface and interactive DT model. The DT is evaluated for loading conditions, but extensions will be introduced to fatigue assessment, already approached by authors in [46] but not generalised for different tyre and wheel families.

Declaration of Competing Interest

The authors declare that they have no known competing financial interests or personal relationships that could have appeared to influence the work reported in this paper.

Data availability

Data will be made available on request.

Acknowledgments

The authors thank D. Rovarino of MW Italia S.r.l for providing the technical material, suggestions and supporting the research in this study. This paperwork is dedicated to the memory of prof. Elvio Bonisoli, a mentor, and a friend, who had contributed to the result achievement of this project.

References

[1] G. Leister, Passenger Car Tires and Wheels: Development - Manufacturing - Application, Springer International Publishing, 2018. ISBN: 978-3-31-950118-5.
[2] Y. Nakajima, Advanced Tire Mechanics, Springer, Singapore, 2019. ISBN: 9789811357992.
[3] A. Tota, L. Dimauro, F. Velardocchia, G. Paciullo, M. Velardocchia, An intelligent predictive algorithm for the anti-rollover prevention of heavy vehicles for off-road applications, Machines 10 (10) (2022) 835, https://doi.org/10.3390/machines10100835.
[4] H.B. Pacejka, I.J.M. Besselink, Tire and Vehicle Dynamics, Elsevier Science, 2012.
[5] ISO 3894:2023 road vehicles - wheels/rims for commercial vehicles - test methods, International Organization for Standardization, Jan. 2023.
[6] E.T.R.T.O. Standards manual, European Tyre and Rim Technical Organisation, 2020.
[7] SAE J2562 biaxial wheel fatigue test, Wheel standards committee, 2021, DOI: 10.4271/J2562_202107.
[8] M. Grieves, Digital twin: manufacturing excellence through virtual factory replication, White paper, 1–7, 2014.
[9] F. Biesinger, B. Kraß, M. Weyrich, A survey on the necessity for a digital twin of production in the automotive industry, in: Proceedings of the 23rd International Conference on Mechatronics Technology (ICMT), 2019, pp. 1–8, https://doi.org/10.1109/ICMECT.2019.8932144.
[10] M. Dal Borgo, S.J. Elliott, M. Ghandchi Tehrani, I.M. Stothers, Virtual sensing of wheel position in ground-steering systems for aircraft using digital twins, model validation and uncertainty quantification, volume 3, in: Proceedings of the Conference Proceedings of the Society for Experimental Mechanics Series, 2020, https://doi.org/10.1007/978-3-030-47638-0_12.
[11] A. Zakrajsek, S. Mall, The development and use of a digital twin model for tire touchdown health monitoring, in: Proceedings of the 58th AIAA/ASCE/AHS/ASC Structures, Structural Dynamics, and Materials Conference, 2017, https://doi.org/10.2514/6.2017-0863.
[12] M.A. de Menezes Lourenço, J.J. Eckert, F.L. Silva, M.H.R. Miranda, L.C.D.A. Silva, Uncertainty analysis of vehicle fuel consumption in twin-roller chassis dynamometer experiments and simulation models, Mech. Mach. Theory 180 (2023), 105126, https://doi.org/10.1016/j.mechmachtheory.2022.105126.
[13] P. Gardner, M. Dal Borgo, V. Ruffini, Y. Zhu, A. Hughes, Towards the development of a digital twin for structural dynamics applications, model validation and uncertainty quantification, volume 3, in: Proceedings of the Conference Proceedings of the Society for Experimental Mechanics Series, 2020, https://doi.org/10.1007/978-3-030-47638-0_18.
[14] J. Yu, Y. Song, D. Tang, J. Dai, A Digital Twin approach based on nonparametric Bayesian network for complex system health monitoring, J. Manuf. Syst. 58 (2021) 293–304, https://doi.org/10.1016/j.jmsy.2020.07.005.
[15] S. Venkatesan, K. Manickavasagam, N. Tengenkai, N. Vijayalakshmi, Health monitoring and prognosis of electric vehicle motor using intelligent-digital twin, IET Electr. Power Appl. 13 (9) (2019) 1328–1335, https://doi.org/10.1049/iet-epa.2018.5732.
[16] R. Magargle, L. Johnson, P. Mandloi, P. Davoudabadi, O. Kesarkar, S. Krishnaswamy, J. Batteh, A. Pitchaikani, A simulation-based digital twin for model-driven health monitoring and predictive maintenance of an automotive braking system, in: Proceedings of the 12th International Modelica Conference. Linköping Electronic Conference Proceedings 132, 2017, pp. 35–46, https://doi.org/10.3384/ecp1713235.
[17] P.K. Rajesh, N. Manikandan, C.S. Ramshankar, T. Vishwanathan, C. Sathishkumar, Digital twin of an automotive brake pad for predictive maintenance, in: Proceedings of the International Conference on Recent Trends in Advanced Computing (ICRTAC) 2019, Procedia Computer Science 165, 2019, pp. 18–24, https://doi.org/10.1016/j.procs.2020.01.061.
[18] C. Cappellini, L. Giorleo, G. Allegri, A. Attanasio, E. Ceretti, A digital twin approach to automotive wheel flow forming process, in: Proceedings of the Managing and implementing the digital transformation. ISIEA 2022 525, Lecture Notes in Networks and Systems, 2022, https://doi.org/10.1007/978-3-031-14317-5_10.
[19] Y. Pan, S. Xiang, Y. He, J. Zhao, A. Mikkola, The validation of a semi-recursive vehicle dynamics model for a real-time simulation, Mech. Mach. Theory 151 (2020), 103907, https://doi.org/10.1016/j.mechmachtheory.2020.103907.
[20] L. He, Y. Pan, Y. He, Z. Li, G. Królczyk, H. Du, Control strategy for vibration suppression of a vehicle multibody system on a bumpy road, Mech. Mach. Theory 174 (2022), 104891, https://doi.org/10.1016/j.mechmachtheory.2022.104891.
[21] M. Gipser, FTire – the tire simulation model for all applications related to vehicle dynamics, Veh. Syst. Dyn. 45 (sup1) (2007) 139–151, https://doi.org/10.1080/00423110801899960.
[22] A. Gallrein, M. Bäcker, CDTire: a tire model for comfort and durability applications, Veh. Syst. Dyn. 45 (sup1) (2007) 69–77, https://doi.org/10.1080/00423110801931771.
[23] F. Ballo, G. Previati, M. Gobbi, G. Mastinu, Tire-rim interaction, a semi-analytical tire model, J. Mech. Des. 140 (4) (2018), https://doi.org/10.1115/1.4038927.
[24] M. Massaro, M. Mottola, E. Bonisoli, D. Lisitano, An experimental procedure for the identification of the dynamic parameters for the rigid-ring tyre model, Meccanica 58 (2023) 981–1001, https://doi.org/10.1007/s11012-023-01654-5.

[25] E. Tönük, Y.S. Ünlüsoy, Prediction of automobile tire cornering force characteristics by finite element modeling and analysis, Comput. Struct. 79 (13) (2001) 1219–1232, https://doi.org/10.1016/S0045-7949(01)00022-0.
[26] W. Hall, J.T. Mottram, R.P. Jones, Tire modeling methodology with the explicit finite element code LS-Dyna, Tire Sci. Technol. 32 (4) (2004) 236–261, https://doi.org/10.2346/1.2186783.
[27] N.D. Korunović, M.D. Trajanović, M.S. Stojković, D. Mišić, J. Milovanović, Finite element analysis of a tire steady rolling on the drum and comparison with experiment, Stroj. Vestn./J. Mech. Eng. 57 (12) (2011) 888–897, https://doi.org/10.5545/sv-jme.2011.124.
[28] X. Yang, Finite element analysis and experimental investigation of tyre characteristics for developing strain-based intelligent tyre system, PhD Thesis, University of Birmingham, Brimingham, UK, 2011.
[29] P. Baranowski, P. Bogusz, P. Gotowicki, J. Małachowski, Assessment of mechanical properties of offroad vehicle tire: coupons testing and FE model development, Acta Mech. Autom. 6 (2) (2012) 17–22.
[30] S. Shokouhfar, S. Rakheja, M. El-Gindy, Development of a computationally efficient rolling truck tyre model using part-composite approach and its verification, Int. J. Veh. Syst. Model. Test. 11 (2) (2016) 142–164, https://doi.org/10.1504/IJVSMT.2016.077929.
[31] X. Wan, Y. Shan, X. Liu, H. Wang, J. Wang, Simulation of biaxial wheel test and fatigue life estimation considering the influence of tire and wheel camber, Adv. Eng. Softw. 92 (2016) 57–64, https://doi.org/10.1016/j.advengsoft.2015.11.005.
[32] F.M. Santiciolli, R. Möller, I. Krause, F.G. Dedini, Simulation of the scenario of the biaxial wheel fatigue test, Adv. Eng. Softw. 114 (2017) 337–347, https://doi.org/10.1016/j.advengsoft.2017.08.006.
[33] E. Bonisoli, D. Lisitano, L. Dimauro, Experimental and numerical mode shape tracing from components to whole motorbike chassis, in: Proceedings of the International Conference on Noise and Vibration Engineering ISMA, Leuven, Belgium, 2018, pp. 3597–3604. September 17-19.
[34] E. Bonisoli, D. Lisitano, L. Dimauro, L. Peroni, A proposal of dynamic behaviour design based on mode shape tracing: numerical application to a motorbike frame, in: Proceedings of the 37th IMAC, A Conference and Exposition on Structural Dynamics, 2020, pp. 149–158, https://doi.org/10.1007/978-3-030-12184-6_14.
[35] E. Bonisoli, D. Lisitano, L. Dimauro, Detection of critical mode-shapes in flexible multibody systems dynamics: the case study of a racing motorcycle, Mech. Syst. Signal Process 180 (2022), 109370, https://doi.org/10.1016/j.ymssp.2022.109370.
[36] M. Firat, R. Kozan, M. Ozsoy, O. Hamdi Mete, Numerical modeling and simulation of wheel radial fatigue tests, Eng. Fail. Anal. 16 (5) (2009) 1533–1541, https://doi.org/10.1016/j.engfailanal.2008.10.005.
[37] E. Bonisoli, C. Rosso, S. Venturini, D. Rovarino, M. Velardocchia, Improvements on design and validation of automotive steel wheels, in: Mechanisms and Machine Science 73, 2019, pp. 1639–1649, https://doi.org/10.1007/978-3-030-20131-9_162.
[38] S. Venturini, E. Bonisoli, C. Rosso, D. Rovarino, M. Velardocchia, Modal analyses and meta-models for fatigue assessment of automotive steel wheels, in: Conference Proceedings of the Society for Experimental Mechanics Series, 2020, pp. 155–163, https://doi.org/10.1007/978-3-030-47638-0_17.
[39] E. Bonisoli, G. Marcuccio, S. Venturini, Interference fit estimation through stress-stiffening effect on dynamics, Mech. Syst. Signal Process 160 (2021), 107919, https://doi.org/10.1016/j.ymssp.2021.107919.
[40] D. Shang, X. Liu, Y. Shan, E. Jiang, Research on the stamping residual stress of steel wheel disc and its effect on the fatigue life of wheel, Int. J. Fatigue 93 (2016) 173–183, https://doi.org/10.1016/j.ijfatigue.2016.08.020.
[41] X. Wan, Y. Shan, X. Liu, T. He, J. Wang, Tire-rim interface pressure of a commercial vehicle wheel under radial loads: theory and experiment, Meas. Sci. Technol. 28 (11) (2017), https://doi.org/10.1088/1361-6501/aa8895.
[42] J.A. Sherwood, B.K. Fussell, W.R. Edwards, T.S. Gross, D.W. Watt, Study of the pressure distribution on an aircraft tire–wheel interface, J. Aircr. 32 (5) (1995) 921–928, https://doi.org/10.2514/3.46819.
[43] K. Cosseron, D. Mellé, J.F. Diebold, F. Hild, S. Roux, Optimized gauging for tire–rim loading identification, Eur. J. Mech. A/Solids 87 (2021) 104–192, https://doi.org/10.1016/j.euromechsol.2020.104192.
[44] J.C. Stearns, T.S. Srivatsan, X. Gao, A. Prahash, P.C. Lam, Analysis of stress and strain distribution in a vehicle wheel: finite element analysis versus the experimental method, J. Strain Anal. Eng. Des. 40 (6) (2005) 513–523, https://doi.org/10.1243/030932405X30786.
[45] J. Van Oosten, H. Unrau, A. Riedel, E. Bakker, Standardization in tire modeling and tire testing—TYDEX workgroup, time project, Tire Sci. Technol. 27 (3) (1999) 188–202.
[46] E. Bonisoli, C. Rosso, S. Venturini, M. Velardocchia, D. Rovarino, L. Actis Comino, M. Baecker, A. Gallrein, A methodology for automotive steel wheel life assessment, in: Proceedings of the WCX SAE World Congress Experience, 2020, https://doi.org/10.4271/2020-01-1240.
[47] E. Bonisoli, C. Rosso, S. Venturini, M. Velardocchia, D. Rovarino, L. Actis Comino, M. Baecker, A. Gallrein, Hardware and virtual test-rigs for automotive steel wheels design, in: Proceedings of the WCX SAE World Congress Experience, 2020, https://doi.org/10.4271/2020-01-1231.
[48] S. Venturini, Design methodologies for automotive steel wheels, PhD thesis, Politecnico di Torino, Torino, Italy, 319, 2022.
[49] G. Fischer, V. Grubisic, Method and apparatus for testing vehicular wheels, U.S. Patent 4-475-383, Oct. 1984.
[50] MTS, Wheel multiaxial fatigue load testing system series 855 - overview of operation, 100-192-743 A, December 2007.
[51] L. Merkx, Overturning moment analysis using the flat plank tyre tester, DCT 2004.078, Technische Universiteit Eindhoven, 2004.
[52] T. Takahashi, M. Hada, K. Oyama, H. Sakai, New model of tire overturning moment characteristics and analysis of their influence on vehicle rollover behavior, Veh. Syst. Dyn. 42 (1–2) (2004) 109–118, https://doi.org/10.1080/00423110412331291517.
[53] D. Lu, K. Guo, H. Wu, N. Moshchuk, X.P. Lu, S.K. Chen, Modelling of tire overturning moment and loaded radius, Veh. Syst. Dyn. 44 (2006) 104–114, https://doi.org/10.1080/00423110600869297.
[54] D. Lu, D. Wang, C. Wang, K. Guo, Tire Carcass Camber and Its Application For Overturning Moment Modeling, SAE International, 2013, https://doi.org/10.4271/2013-01-0746.
[55] M. Guiggiani, The Science of Vehicle Dynamics: Handling, Braking, and Ride of Road and Race Cars, Springer International Publishing, 2018. ISBN: 978- 3-31-973220-6.
[56] E. Bonisoli, C. Delprete, C. Rosso, Proposal of a modal-geometrical based master nodes selection criterion in modal analysis, Mech. Syst. Signal Process 23 (3) (2009) 606–620, https://doi.org/10.1016/j.ymssp.2008.05.012.
[57] E. Bonisoli, L. Dimauro, S. Venturini, Lupos: open-source scientific computing in structural dynamics, in: Proceedings of the 41st IMAC, A Conference and Exposition on Structural Dynamics, Austin, Texas, USA, 2023.